Fuel 372 (2024) 132257

Contents lists available at ScienceDirect

Fuel

journal homepage: www.elsevier.com/locate/fuel

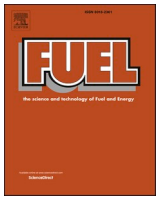

Full Length Article

Experimental investigation for enhancing the performance of hydrogen direct injection compared to gasoline in spark ignition engine through valve timings and overlap optimization

Mohamed Mohamed [a,*], Abinash Biswal [a], Xinyan Wang [a], Hua Zhao [a], Jonathan Hall [b]

[a] Brunel University, United Kingdom
[b] Mahle Powertrain, UK

ARTICLE INFO

Keywords:
Hydrogen direct injection
Variable valve timing vs H2ICE

ABSTRACT

Recent advances in hydrogen internal combustion technologies highlight its potential for high efficiency and zero carbon emissions, offering a promising alternative to fossil fuels. This paper investigates the effects of valve timings and overlaps on engine performance, combustion characteristics, and emissions in a boosted direct-injection single-cylinder spark ignition engine using both gasoline and hydrogen. Optimized direct hydrogen injection effectively eliminates backfires and hydrogen slip during positive cam overlaps, significantly reducing the pumping mean effective pressure. The study's primary finding demonstrates the potential of hydrogen to operate as a direct substitute for a gasoline engine without necessitating changes to the cam profiles at the high load operation. Furthermore, the study demonstrates that hydrogen leads to much higher thermal efficiencies across a wider range of engine loads when operated at a lean, air-to-fuel ratio of 2.75. The engine operating with such a lean-burn hydrogen mixture keeps the engine-out NOx emission at ultra-low levels. Compared to gasoline, hydrogen exhibits greater stability and a reduced reliance on camshaft timing during engine operation.

1. Introduction

Fossil fuels, such as petrol and diesel, have long been the cornerstone of global transportation and energy production [1,2,3]. However, their combustion is a major source of atmospheric pollutants, including carbon dioxide (CO_2), nitrogen oxides (NOx), and particulate matter, contributing significantly to air pollution and climate change. Gaseous fuels are expected to overtake liquid fuels as the preferred Fuel in the near future, owing to growing worries about climate change and the need for sustainability [4,5,6]. Reports from worldwide economic institutions show that we are on track to enter a "hydrogen era" within the next few decades [7,8]. This change is driven by the awareness of hydrogen's promise as a clean and adaptable energy carrier, providing solutions in various industries, including transportation, manufacturing, and power generation. Advancements in hydrogen generation, storage, and use technologies, together with increased investments and regulatory backing, make the idea of a hydrogen-based economy more possible. This change promises to revolutionize energy systems, enabling a move to a greener, more robust, more sustainable future [9].

As the worldwide push to attain net zero carbon emissions grows, the automotive sector encounters tremendous pressure to innovate and move away from conventional fossil fuels [10,11]. In this perspective, hydrogen stands out as a highly attractive choice for decarbonizing transportation, with zero-emission potential when produced from

Abbreviations: **10%to90%BurnDuration**, **Burn Duration**; **50%MB (CA50)**, **Combustion Phasing at 50% burn**; **AFR / λ**, **Relative Air-Fuel Ratio**; **ATDCf/g**, **After the Top Dead Centre firing/gas exchange**; **BEV**, **Battery Electric Vehicle**; **BTDCf/g**, **Before the Top Dead Centre firing/gas exchange**; **BTE**, **Brake thermal efficiency**; **BP valve**, **Back pressure valve**; **CAD**, **Crank Angle Degree**; **CO**, **Carbon Monoxide**; **CO_2**, **Carbon Dioxide**; **COV_{IMEP}**, **Coefficient of Variation of IMEP**; **DAQ**, **Data Acquisition**; **DI**, **Direct Injection**; **ECU**, **Electronic Control Unit**; **EGR**, **Exhaust Gas Recirculation**; **FCEV**, **Fuel Cell Electric Vehicle**; **GHG**, **Greenhouse Gas**; **H_2**, **Hydrogen**; **HC**, **Hydrocarbons**; **ICE**, **Internal Combustion Engine**; **IMEP**, **Indicated Mean Effective Pressure**; **ITE**, **Indicated Thermal Efficiency**; **IPCC**, **Intergovernmental Panel on Climate Change**; **LNV**, **Lower Net Value**; **NH_3**, **Ammonia**; **NOx**, **Nitrogen Oxides**; **O_2**, **Oxygen**; **PFI**, **Port Fuel Injection**; **PLC**, **Programmable Logic Controller**; **PID**, **proportional integral derivative**; **PPM**, **Particulate Per Milone**; **PMEP**, **Peak Mean Effective Pressure**; **SI**, **Spark Ignition**; **Sparkto10%BurnDuration**, **Crank angle of 10% mass burn**.

* Corresponding author at: Centre for Advanced Powertrain and Fuels, College of Engineering, Design and Physical Sciences, Brunel University London Uxbridge UIB8 3PH, United Kingdom.

E-mail address: moahmed.mohamed@brunel.ac.uk (M. Mohamed).

https://doi.org/10.1016/j.fuel.2024.132257
Received 19 April 2024; Received in revised form 2 June 2024; Accepted 14 June 2024
Available online 20 June 2024

renewable sources. The appeal of hydrogen internal combustion engines (H2ICE) arises from their potential to capitalize on the advanced state of internal combustion engine (ICE) technology, such as reliability, durability, existing supply chains, manufacturing infrastructure, and cost-effectiveness. This establishes H2ICE as a realistic and widely applicable solution for expediting hydrogen integration into the transportation sector, both in the short and long term. Leveraging the existing global expertise in ICEs and established manufacturing and supply chains ensures a smooth transition without significant disruptions [12,13]. Furthermore, H2ICE technology can be more cost-effective and reliable for various applications than fuel cell technologies. Additionally, by using the same manufacturing facilities and procedures as conventional ICEs, H2ICEs help to ensure job stability and long-term economic prospects in the automotive sector.

Hydrogen has unique thermochemical characteristics that present opportunities and challenges for its use in the IC engine Hydrogen, being the lightest molecule, exists in a gaseous state. This characteristic results in its lower density compared to liquid fossil fuel, necessitating a larger volume of hydrogen fuel to store an equivalent amount of energy [14]. The high diffusivity of hydrogen facilitates rapid mixing, yet it can pose challenges for injector sealing [15]. Hydrogen has a viscosity one to two orders lower than conventional fossil fuels, making it difficult to decrease friction and dampen the injector needle [16]. Hydrogen fuel's faster burning velocity and wide flammability range enhance stable combustion over a wide range of air to fuel ratios, eliminating concerns about partial burning and misfire [17], improving the overall efficiency and near zero NOx emission through ultra lean-burn combustion of hydrogen engines [18,13]. Hydrogen has a low ignition energy, increasing the chances of surface ignition or backfire. Another concern is hydrogen leakage into the crankcase [19]. Low activation energy can result in ignition inside the crankcase. A possible solution to the problem is to minimize blow-by to keep hydrogen concentrations below the flammability limit over time, such as by ring packages and crankcase additional scavenging. Hydrogen has a higher burning velocity compared to conventional gasoline fuel [20,21,22] At high load operations, its high laminar lame speed can lead to a rapid pressure rise rate and very high peak cylinder pressure. Moreover, hydrogen demonstrates superiority in emission levels, combustion stability, and lean limit when utilized in internal combustion engines (ICEs) compared to any other fossil fuels [23,24,25,26]. As a non-toxic and carbon-free gas, hydrogen does not contribute to the emissions of unburned hydrocarbons (HC) and carbon oxides, thereby guaranteeing significant reductions in pollution from ICEs [27].

Numerous studies have highlighted that direct injection of hydrogen into the engine cylinder outperforms the port-fuel injected engine operation in terms of reducing engine backfires [28,29,30]. Researchers have made various attempts to convert conventional direct injection (DI) gasoline engines into hydrogen-fueled engines through a range of modifications while carefully considering the unique properties of hydrogen. Sopena et al. [31] converted a commercial SI engine (Volkswagen Polo) to run on hydrogen by modifying the inlet manifold, injectors, and oil radiator. Operating successfully under lean air-hydrogen mixtures (λ: 1.6–3.0), the engine showed no unfavourable behaviours like knocks or backfires. Hydrogen-fueled engines exhibited significantly higher brake thermal efficiency (BTE) compared to gasoline, with sufficient power to reach a maximum vehicle speed of 140 km/. Lee et al. [32] developed a single-cylinder SI hydrogen research engine with double overhead cams, mechanical continuous variable valve timing (MCVVT), and supercharger systems. This configuration aimed to achieve high-power performance while minimizing emissions. It was reported that the backfire occurrence might be controlled by delaying the intake valve opening (IVO) timing. Retarding the IVO to the top dead centre (TDC) resulted in no backfire during the natural intake engine operating from a lean mixture up to lambda of 1.4. Fine et al. [33] modified a Ford V-8 spark ignition (SI) engine into a hydrogen engine. They modified the engine to include a custom cam, injection system, and computer control unit. Despite encountering pre-ignition, the engine, operating at a compression ratio of 12:1, produced very low NO_x emissions of less than 12 ppm.

Direct injection of hydrogen into spark ignition engines helps to avoid the backfire without the need to minimize the valve overlap. However, the camshaft timing and valve overlap still affect the engine performance and efficiency. Camshaft timing influences the opening and closing of the intake and exhaust valves and valve overlap, which is the period when both intake and exhaust valves are open simultaneously, substantially impacting engine combustion and efficiency. While considerable progress has been made in advancing hydrogen engine technologies, significant gaps remain in understanding the optimal engine configurations for maximizing efficiency and reducing emissions. Specifically, there is a lack of comprehensive studies examining the influence of valve timing and overlap on the performance of hydrogen-fueled engines compared to traditional gasoline engines. This research seeks to fill this gap by exploring how variations in valve timings can enhance the efficiency, stability, and emissions profile of hydrogen engines, providing crucial insights for the development of more sustainable internal combustion engine technologies.

2. Experimental setup

The experimental configuration for hydrogen engine operation requires significant modifications. One of the primary challenges of hydrogen fuel is determining the special risk assessments for the hydrogen supply system. The proper operation of the engine test cell using hydrogen necessitates a safe, long-term, and permanent location for storing hydrogen bottles while avoiding any potential hazards within the test cell. To address these concerns, the preferred solution is to securely isolate and adequately ventilate the hydrogen bottles outside the test cell in a confined space without a ceiling and surrounded by fire shields.

Furthermore, it is decided to locate all supply line accessories, including pressure regulators, sensors, flow meters, and shutdown valves, outside the test cell. This approach significantly minimizes the potential risk of leakage within the test cell. The test cell has an additional air ventilation system with a flexible hood above the engine and additional suction gills next to the ceiling. Besides, the engine test cell has been installed with hydrogen sensors linked to an automated shutdown Programmable Logic Controller (PLC) system. This system is designed to respond automatically by shutting off the hydrogen supply if any hydrogen sensors detect levels exceeding 3 %, including a hydrogen sensor that detects the potential accumulation of hydrogen in the crankcase ventilation system. A double pipe installation with an integrated nitrogen purging system ensures that any leaked hydrogen remains uncontaminated within the test cell environment. A pressure sensor is connected to the PLC to facilitate this process, activating a purging nitrogen system.

2.1. Single cylinder SI engine

This study was carried out on a state-of-the-art SI single-cylinder engine originally designed for boosted direct injection gasoline operation, which has been adopted to operate with both direct hydrogen injection and port fuel injection. Although either centrally-mounted or side-mounted direct injection injectors had been used, the present study was carried out with the centrally-mounted injectors for hydrogen and gasoline operations. A DI-CHG10 injector from Phinia was utilized for H2 engine operation, capable of hydrogen injection from 10 to 40 bar in the DI system. The engine was controlled by an adaptable MAHLE electronic control unit (ECU), allowing seamless switching between hydrogen and gasoline without significant control system adjustments. The engine is equipped with fully variable valve timings for both intake and exhaust valves, enabling flexibility in determining the optimal overlap configuration for different engine operating conditions. The

ECU allows adjustment of the injection time and pressure, providing the ability to modify the start or end of the injection process as needed. The engine was supplied with compressed air by an external compressor. The intake pressure is regulated by an external proportional integral derivative (PID) pressure controller and an air heater, both accurately controlling the intake pressure and temperature. When dealing with a single-cylinder engine, it is essential to accurately identify and calculate the necessary amount of back pressure required for higher boost levels to achieve precise results representative of the turbocharged SI platforms. To ensure this, we have incorporated a venturi in the exhaust pipe to simulate the exhaust pressure in a turbocharged engine and avoid water condensation in the exhaust pipe to protect the emission analyzers.

The engine's main specifications are presented in Table 1. Fig. 1 illustrates the configuration of the single-cylinder engine test setup and Fig. 2 shows the design of the combustion chamber, locations of the spark plug and the DI injector in the cylinder head.

An inline air heater with PID control maintained a constant intake temperature of 38 degrees Celsius. Additionally, the oil and water coolant temperatures were kept constant at 90 °C with the help of external heaters.

2.2. Data acquisition and analysis

The test cell being analyzed consists of 138 sensors that require monitoring and record-keeping of their readings. The sampling rate for each sensor is determined based on its priority and the value of the reading it produces. In particular, the instantaneous in-cylinder, intake, and exhaust pressures are recorded at a high sampling rate of 0.25 Crank Angles. In contrast, the outputs from static pressure and temperature sensors are recorded much slower in the regular time domain. A hybrid selection of fast and standard USB NI cards was utilized to accommodate this, which can auto-synchronize with the Ni-based combustion analyzer supplied by Valieteck [35]. Furthermore, a NI-to-CanBus communication card was used to transfer signals from the ECU.

The indicated thermal efficiency is calculated by dividing the indicated power by the product of the fuel's flow rate and its lower heating value. The in-cylinder pressure readings dictate the indicated power, averaged over 300 cycles, as shown in Eq. (1).

$$ITE(\%) = \frac{IndecatedPower(kW) \times 3600}{Fuelflow\left(\frac{kg}{hr}\right) \times \text{CalorificValue}\left(\frac{kJ}{kg}\right)} \quad (1)$$

Table 1
Engine specs [33].

Configuration	Single cylinder
Displaced volume	400 cc
Stroke X Bore	73.9 mm x 83 mm
Compression Ratio	11.3: 1
Number of Valves	2 intake and 2 exhaust
Exhaust Valve Timing	EMOP (Exhaust Maximum Opening Point) 100-140°CA BTDCg, Maximum valve lift 11 mm, 278 °CA Total Duration
Inlet Valve Timing	IMOP (Intake Maximum Opening Point) 80–120 °CA ATDCg, Maximum valve lift 11 mm, 240°CA Total Duration
Injection Control	MAHLE Flexible ECU (MFE)
Spark location	Top central toward exhaust valves
Spark Plug Type	Surface Discharge Type (NGK HR10)
Combustion Chamber configuration	Tumble-based (NDRT 0.7 @ max lift)
Piston Shape	Central Bowl Style
Injector spray	8-hole centrally mounted GDI injectors (For gasoline injection)Outward opening hollow cone spray formation (For H_2 Injection)
Injector Position	Top central toward inlet valves

The variability in combustion cycles was measured by COV_{IMEP}, the coefficient of variation of the indicated mean effective pressure over 300 cycles as given by Eq. (2). The lower net value (LNV) is also introduced to detect partial combustion or misfiring events. The calculation of LNV is based on the ratio of the peak in-cylinder gas pressure to the average peak pressure for 300 cycles, as shown in Eq. (3).

$$COV_{IMEP}(\%) = \frac{\sqrt{\frac{\sum_{i=1}^{n}(IMEP_i - IMEP_{mean})^2}{n-1}}}{IMEP_{mean}} \quad (2)$$

$$LNV_{min}(\%) = \frac{Peakin-cylinder(Kpa)_{min}}{Peakin-cylinder(Kpa)_{av}} * 100 \quad (3)$$

Two methods were used to detect the Top Dead Centre (TDC): the encoder clock synchronized with the peak in-cylinder pressure during the motoring phase and a hole-effect sensor attached to the crankshaft, which the ECU used to regulate the cam timing.

The pegging pressure was measured by determining the intake pressure value at the valve opening stage, which was then offset in the in-cylinder pressure live data obtained from the DAQ system.

Monitoring the engine-out emissions is critical to capture and understand the engine emission patterns through different hardware starting from the steady state HORIBA (MEXA-584L) that continuously measures CO/CO_2 and O_2 [36]. Signal Instruments analyzers measured the hydrocarbon (HC) and NO_x emissions based on flame ionization detection (FID) and chemiluminescence methods. In addition, a fast response Cambustion NO_x analyzer was employed for the fast NO_x emission measurement by sampling the exhaust gas in the back of the exhaust valves with a 1.2-meter emission pipe to reduce the delay of the NO, NO_2 measurements [37]. Finally, a V&F hydrogen analyzer was installed to measure hydrogen concentration in the engine exhaust or the ventilated crankcase line [38].

Two wide-band lambda sensors were used and positioned in the exhaust line to determine lambda values. These sensors were calibrated using O_2 measurements obtained from the Horiba emission analyzers. Finally, the measured values of the lambda sensors were checked with those calculated from the exhaust gas analyzers.

3. Test methodology

The engine was fueled with either pure hydrogen or EU VI gasoline (95 RON E10, containing 10 % ethanol). The engine was operated at a fixed load of 1000 KPa IMEP and a constant speed of 2000 rpm, representing the mid-load and speed of the engine operating map. Although the hydrogen fuel's operating range spans from lambda 1 to 5, the lambda selected for this study was determined to be 2.75 based on targeting the peak ITE with the minimum boost required while maintaining NOx emissions at a low level [39]. On the other hand, gasoline has been shown to operate with higher stability at lambda 1. The combustion phasing (50 % MFB/CA50) was kept between 8 and 10 CAD_{ATDCf} by setting the spark timing to the maximum brake torque (MBT).

Fig. 4 shows the maximum and minimum valve overlap that can result from altering each valve's valve timing as well as the duration of the intake and exhaust valves. Moving both the intake and exhaust valves by 40 crank degrees is possible, eliminating the overlap or allowing for a maximum overlap duration.

Table 2 presents the testing conditions for both fuels during the cam matrix studies. This information will prove valuable for analyzing and comparing the results and useful for addressing the study's outcomes. Table 3 provides information about the key properties of gasoline and hydrogen.

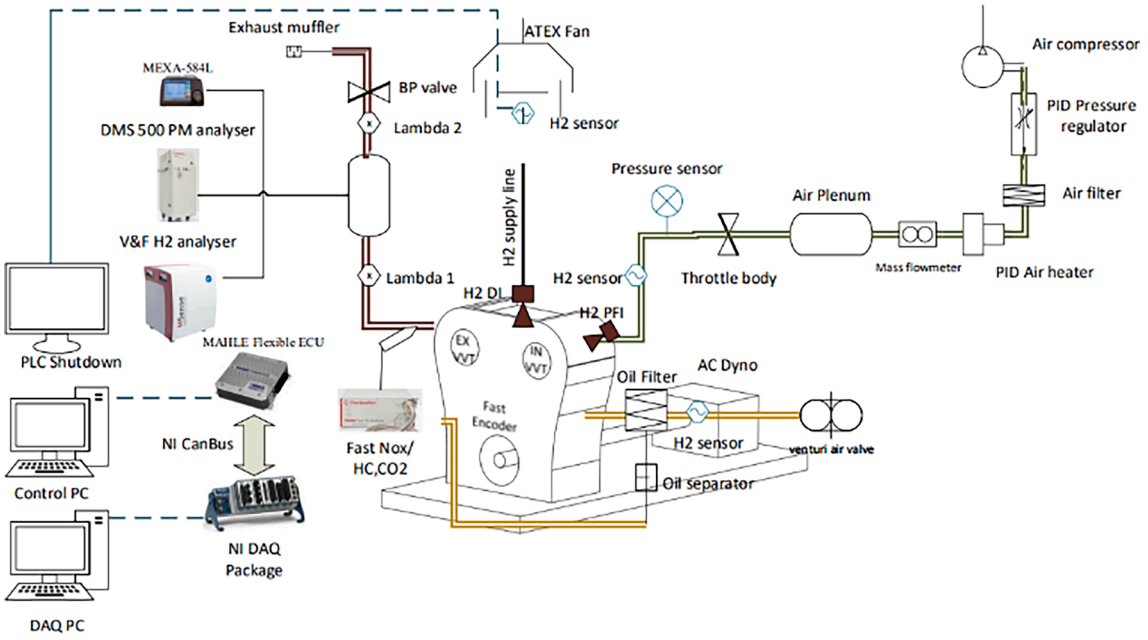

Fig. 1. Testbed schamtic [34].

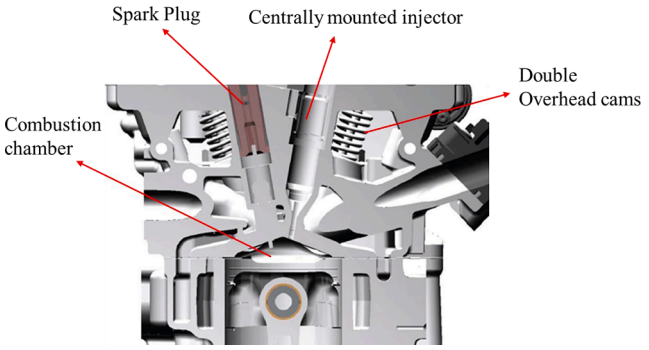

Fig. 2. Combustion configuration.

4. Results and discussions

The results are presented as 2D maps to illustrate how the intake and exhaust valve opening timings affect the engine's efficiency, performance and emissions. Fig. 5 compares the variations of indicated thermal efficiencies (ITE) with the valve timings. The x-axis is the crank angle of the maximum exhaust valve opening, and the exhaust valves are opened earlier (more advanced) from left to right. The y-axis is the crank angle of the maximum intake valve opening, and the opening of the intake valve are delayed from 75 to 115 CA ATDC. Therefore, the overlap ratio is increased from zero in the top right corner to the maximum in the bottom left corner, as indicated by the blue arrow. Overall, hydrogen shows much higher thermal efficiencies than gasoline across the whole range of operations, primarily thanks to the lean-burn hydrogen combustion at a higher lambda of 2.75. It is worth noting that this has been achieved in an engine that is optimized to operate with gasoline.

Fig. 5 shows that the hydrogen engine's thermal efficiency is almost independent of the valve timing and the valve overlap for the fixed fuel injection timing of 150 CA BTDC at the start of the compression stroke. The gasoline engine exhibits a slightly higher thermal efficiency when the maximum opening of the exhaust valves is at 102 CA BTDCg with some valve overlap.

Fig. 6 compares the first part of the combustion process of hydrogen and gasoline fuels as measured by the 10–50 % mass fraction burned. The results show that hydrogen fuel burns slower by around 4–5 crank angles than gasoline fuel due to the much higher relative air-to-fuel ratio of 2.75 compared to stoichiometric gasoline combustion. In the case of the gasoline engine, the 10 %–50 % burn duration increases slightly as the intake valve opening takes place earlier, but it is not affected by the exhaust valve timings. Hydrogen fuel, on the other hand, exhibits a slightly shorter burn duration when operated in the maximum overlap region in the bottom left.

Fig. 7 shows that the second half of the combustion process, as measured by the 50–90 % burn duration, is faster than the first part of the combustion process by several CAs, as more fuel can be burnt in the fully developed flame front. This is more pronounced in hydrogen combustion than the gasoline combustion. The 50 %–90 % burn duration of gasoline combustion remains constant, whilst that of hydrogen combustion exhibits slightly slower combustion when both intake and exhaust valve opening times are in the middle with an intermediate valve overlap period.

As shown in Fig. 8, the total burn duration of hydrogen is about 7–8 degrees slower than gasoline and is slightly more affected by the valve timings and valve overlap period. In the region with large valve overlap (bottom left), hydrogen exhibits faster burn durations by 2 degrees whilst gasoline experiences slower burn durations. This could be caused by the variation of mixture formation due to the interactions between the fuel injection and the airflow. Hydrogen is injected at 30 bar at 150 degrees BTDCf as a gaseous fuel, and gasoline is injected s at 100 bar at 350 degrees BTDCf as a liquid fuel. Further studies are needed to understand how the mixture formation process of hydrogen can be affected by the engine operating conditions, such the valve timings, injection timings and injection pressures.

For completeness, Fig. 9 shows the spark timing contours for both hydrogen and gasoline engines. As the target CA50 is set to about 8–10 CA ATDC for maximum output and efficiency, more advanced spark timings are needed for hydrogen engine operation to compensate for the slower flame speed of the ultra-lean-burn mixture.

Fig. 10 depicts the Pumping Mean Effective Pressure (PMEP) trend, a vital element to consider, particularly in lean operating conditions. Hydrogen needs a higher intake pressure and shows positive PMEP values. The negative PMEP values of gasoline indicate the intake is still operating at slightly below the ambient pressure. Additionally, it should

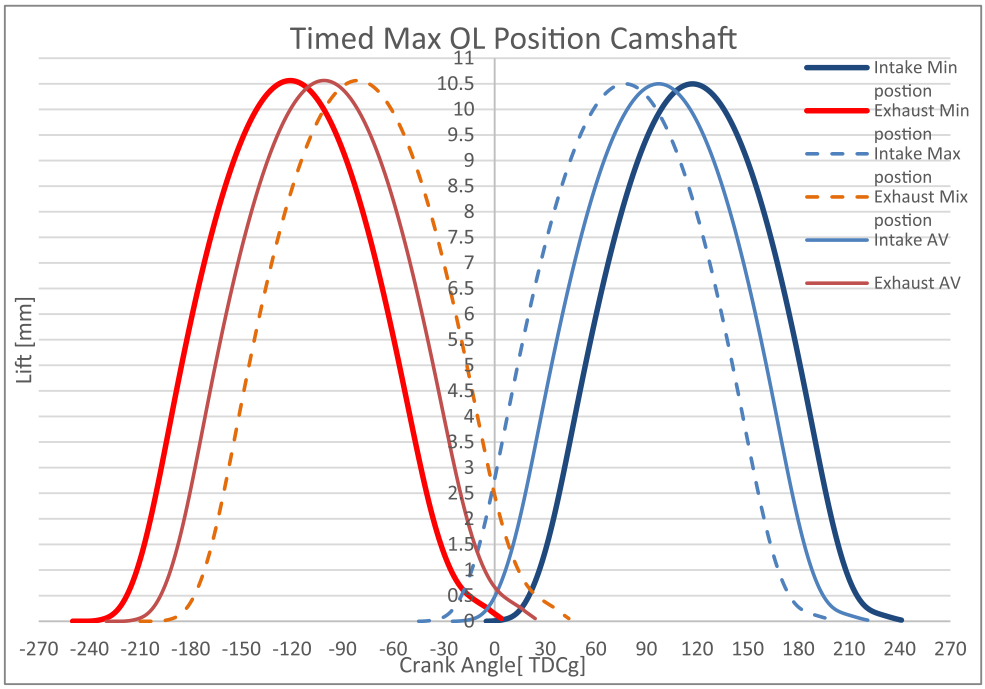

Fig. 4. Intake and Exhaust cam profile with maximum and minimum overlap.

Table 2
Engine test conditions.

Engine parameters	Unit	Cam envelope sweep test
Engine Speed	rpm	2000
Engine Load	kPa	1000
Lambda (λ)	–	2.75for hydrogen, 1.0 for gasoline
Intake Cam positions	ATDCg	SWEEP (between 117 and 77 degrees with 5 degrees increment)
Exhaust Cam positions	BTDCg	SWEEP (between 122 and 82 degrees with 5 degrees increment)
Start of injection for hydrogen DI	BTDCf	150
Start of injection for gasoline DI	BTDCf	350
Injection pressure for hydrogen DI	kPa	3000
Injection pressure for gasoline DI	kPa	10,000
50 % mas burn (CA50)	CAD_{ATDCF}	8
Air intake temperature	c	38

Table 3
Comparison of fuel proprieties between Hydrogen and Gasoline [40,41].

Properties	Units	Hydrogen	Gasoline
Auto-ignition Temperature	K	858	550
Lower heating value	MJ/kg	119.93	44.2
Density	Kg/m^3	0.08	730
Molecular weight	g/mol	2.016	60–150
Flammability limits in air	vol%	4–75	1.4–7.6
Flame velocity	m/s	2.65–3.25	0.37–0.43
Specific gravity	–	0.091	0.71
Boiling point	K	20.2	230
Octane number	–	130	95
Mass diffusivity in air	cm^2/s	0.61	0.89
Adiabatic flame temperature (at stoichiometry)	K	2480	2580
Minimum ignition energy (at stoichiometry)	mJ	0.02	0.24
Stoichiometric fuel/air mass ratio	–	0.029	0.068
Flame velocity (at stoichiometry)	m s^{-1}	1.85	0.26

be noted that the exhaust pressure was elevated above the ambient pressure due to the presence of a venturi in the exhaust pipe.

Gasoline's PMEP is mostly affected by the exhaust valve timing, and it decreases by 6 KPa from the earliest to the most retarded exhaust opening, leading to a higher volumetric efficiency. Conversely, the hydrogen engine is characterized by higher PMEP with more retarded exhaust timing, resulting in higher boost pressure. Additionally, the positive PMEP decreases from the top right (minimum valve overlap) to the bottom left (maximum valve overlap), and hence, less intake air boosting is required.

Fig. 11 presents data that evaluate the engine's stability across 300 cycles and its variation with the valve timings, as measured by the coefficient of variation of IMEP. The results show that both engines can be operated smoothly with very small cycle-to-cycle variations of <2 %. Due to the very lean-burn combustion, hydrogen fuel has a slightly greater variability than gasoline. Moreover, gasoline fuel depends on the valve timing, with higher fluctuations of 1.3 % across the matrix. In contrast, hydrogen fuel displays fewer fluctuations of COV_{IMEP}, with the lowest value observed at maximum overlap.

Fig. 12 showcases an aspect that determines the steady-state's lower net value (LNV) at 10 bar IMEP for 300 cycles to evaluate the combustion process's stability and consistency in each cycle. This parameter is used to determine the smallest partial combustion value over the 300 cycles to the average data. Regardless of the valve timing, the LNV for both fuels indicates highly reliable combustion. Gasoline fuel exhibits greater parietal burn, as shown by its slightly lower LNV than hydrogen. The cam matrix fluctuation shows lower LNV values in gasoline than in hydrogen. Hydrogen has a minimum of 95 % value and gasoline is at a lower value of 92 %. While hydrogen exhibits slightly higher COV_{IMEP} by 0.8 %, it demonstrates more consistent combustion over the 300 cycles with an LNV of 3 % higher than gasoline.

Fig. 13 presents the indicated power of both fuels over the valve timing matrix. The data shows almost the same indicated power for both fuels. At the same time, the hydrogen experiences a higher variation in the indicated power due to the slightly higher error gain in the wide band lambda sensor. That's due to the O2 emission out characteristics, which results in a magnification of the error gain for targeting learn combustion strategy, which influences the variation due to the target

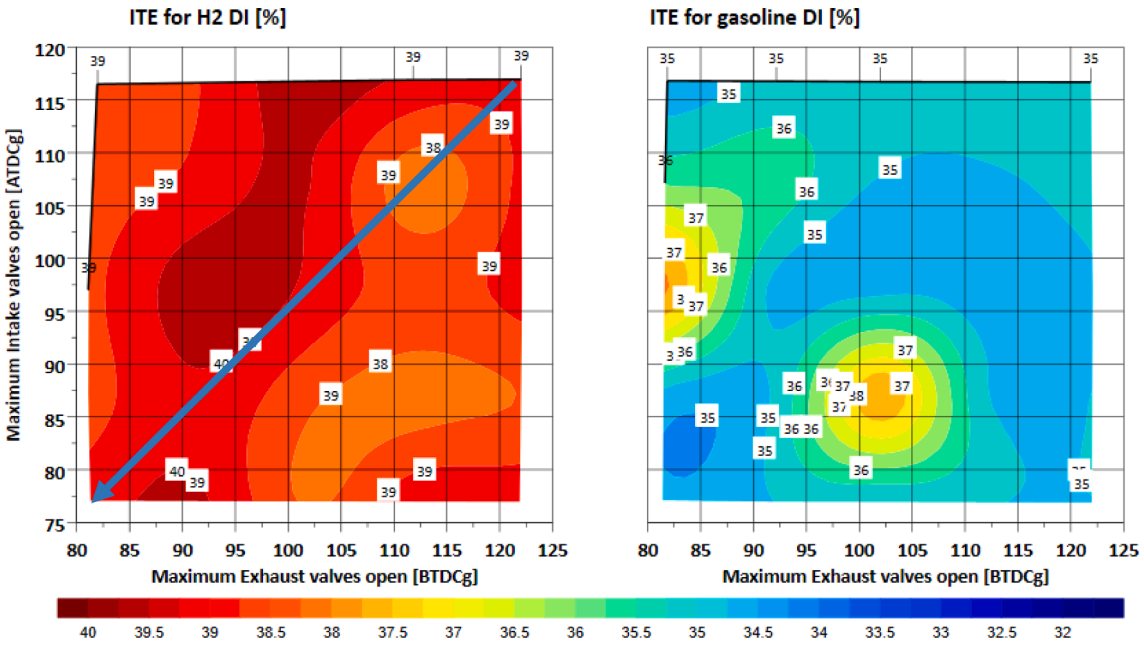

Fig. 5. The indicated thermal efficiency (ITE) for hydrogen and gasoline engines at 10 bar IMEP and 2000 rpm.

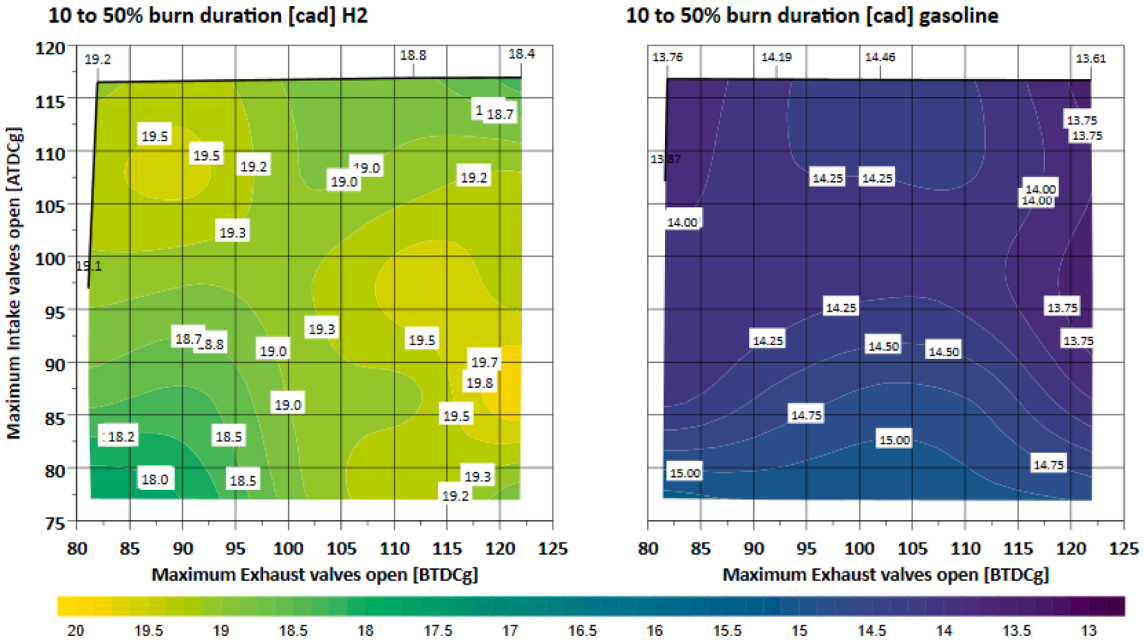

Fig. 6. 10–50 % burn durations for hydrogen and gasoline engines at 10 bar IMEP and 2000 rpm.

operation of lambda 2.75.

Fig. 14 depicts the primary engine-out emissions of hydrogen and gasoline, specifically focusing on NO_x emissions. Since hydrogen is a zero-carbon fuel, the standard emission analyzers detected zero CO2, CO, and HC emissions in the engine's exhaust. However, a tiny amount of CO2/CO and HC could be produced if the lubrication oil enters the combustion chamber either through the piston rings or crankcase ventilation.

The hydrogen engine is characterized by ultra-low NO_x emissions below 100 pm, due to the low gas temperature of the ultra-lean-burn combustion at lambda 2.75. Compared with the gasoline engine, this represents a 94 % reduction in the engine's NOx emissions.

In the context of hydrogen engine operation, we observed that the highest NOx emission of 110 ppm is detected when the engine operates with the maximum valve overlap, the most retarded exhaust timing, and the most advanced intake valve timings. Additionally, we noticed that a greater difference in engine pressure leads to higher NOx emissions due to the increased boosting pressure necessary to achieve a lambda value of 2.75. On the other hand, when it comes to gasoline NOx engine-out emissions, we found that lower NOx reduction occurs in the maximum overlap region. This is because NO is primarily formed in areas with high combustion gas temperatures exceeding 1800 K. The variation in NOx emissions with valve timings and valve overlap is likely linked to an inhomogeneous mixture in the hydrogen engine, resulting in higher combustion temperatures in the slightly fuel-rich mixture within an overall ultra-fuel-lean mixture. This could also explain the marginally faster combustion and shorter burned duration observed when the hydrogen engine is operated with a larger valve overlap, as indicated in

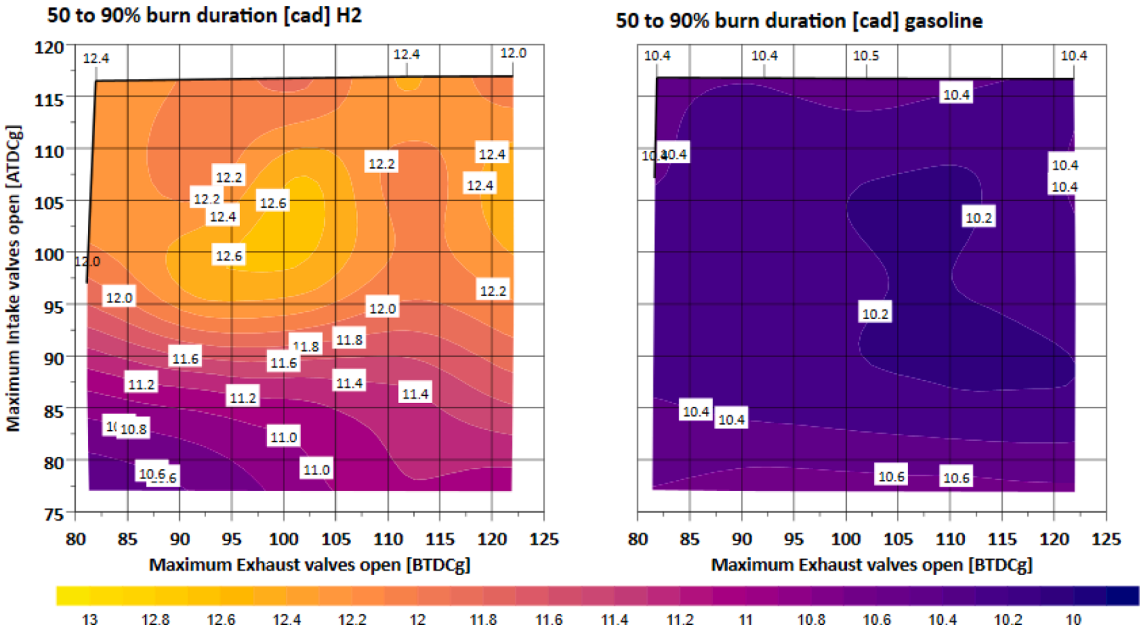

Fig. 7. 50–90 % burn durations for hydrogen and gasoline engines at 10 bar IMEP and 2000 rpm.

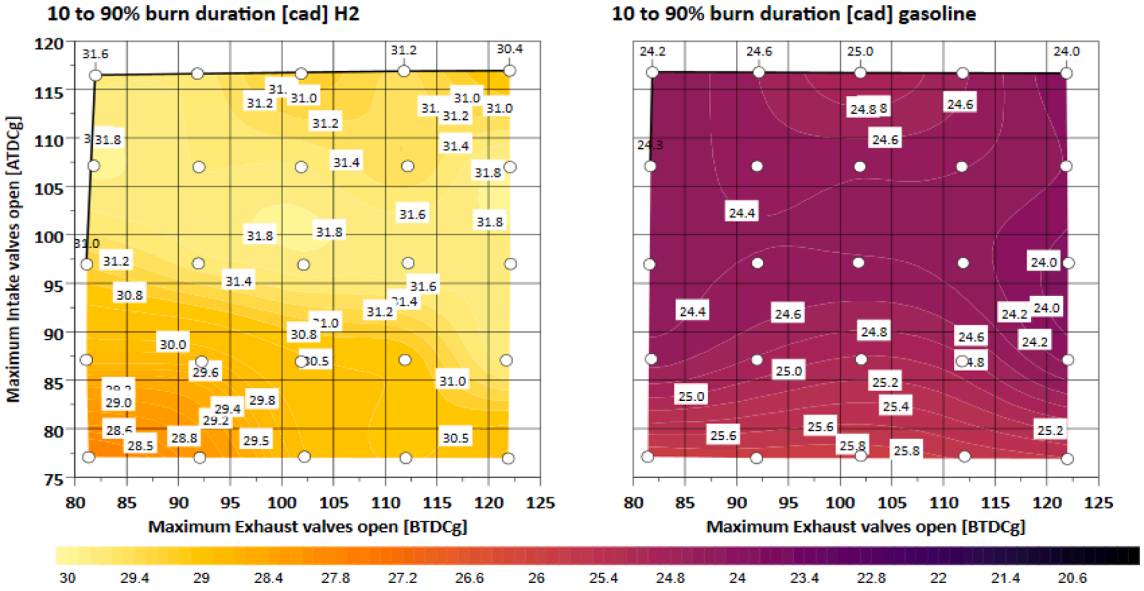

Fig. 8. 10–90 % burn durations for hydrogen and gasoline engines at 10 bar IMEP and 2000 rpm.

Fig. 8.

Fig. 15 compares the emissions of unburnt fuels as H2 slip from the hydrogen engine and the unburned hydrocarbons from the gasoline engine. The gasoline engine produces an average of 272 ppm of unburnt hydrocarbon emissions. While the hydrogen engine produces no carbon emissions, it generates an average of 442 ppm of hydrogen slip in the engine exhaust. The H2 slip increases with the more advanced intake valve opening and reaches its maximum at the average exhaust opening time with a very early intake opening region. Similar trends can be seen for the unburnt HCs from the gasoline engine.

5. Conclusion

A comprehensive investigation was carried out on the effect of valve timings, and valve overlaps on the engine's performance, efficiency, combustion and emissions from a single-cylinder spark ignition engine operated with direct injection gasoline and hydrogen. As hydrogen is injected directly into the cylinder, maximum valve overlap can be used without encountering any backfires as it would have in a port injection hydrogen engine. The study was carried out at a mid-load of 10 bar IMEP and a constant engine speed of 2000 RPM by setting the spark timing to the MBT (Minimum ignition advance for Best Torque) and CA50 at 8–10 CA ATDC. The injection timing is fixed at 150 CA BTDC at the start of the compression stroke.

The results are presented in the form of contours of Indicated Thermal Efficiency and ISFC, combustion durations and cyclic variations, PMEP, and emissions of NO_x and unburnt fuels (HC/H2 slip). The main findings are summarised as follows:

1- Using a single-cylinder spark ignition engine designed and optimized for gasoline, it is shown that the engine, when fuelled with hydrogen, demonstrates a significantly higher thermal efficiency by 5 % than

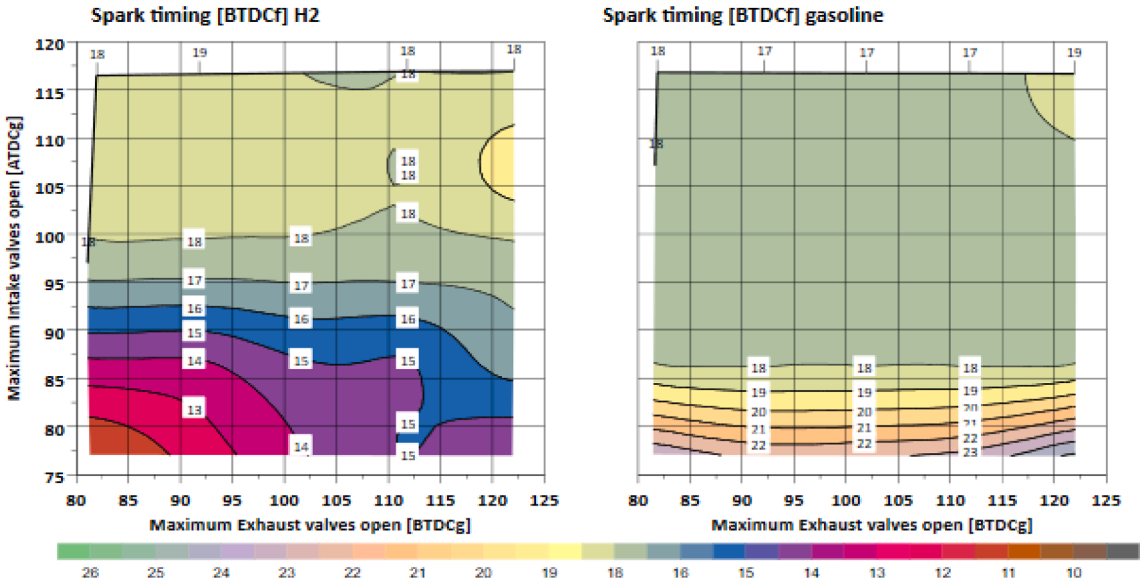

Fig. 9. The Spark timing [BTDCf]for hydrogen and gasoline engines at 10 bar IMEP and 2000 rpm.

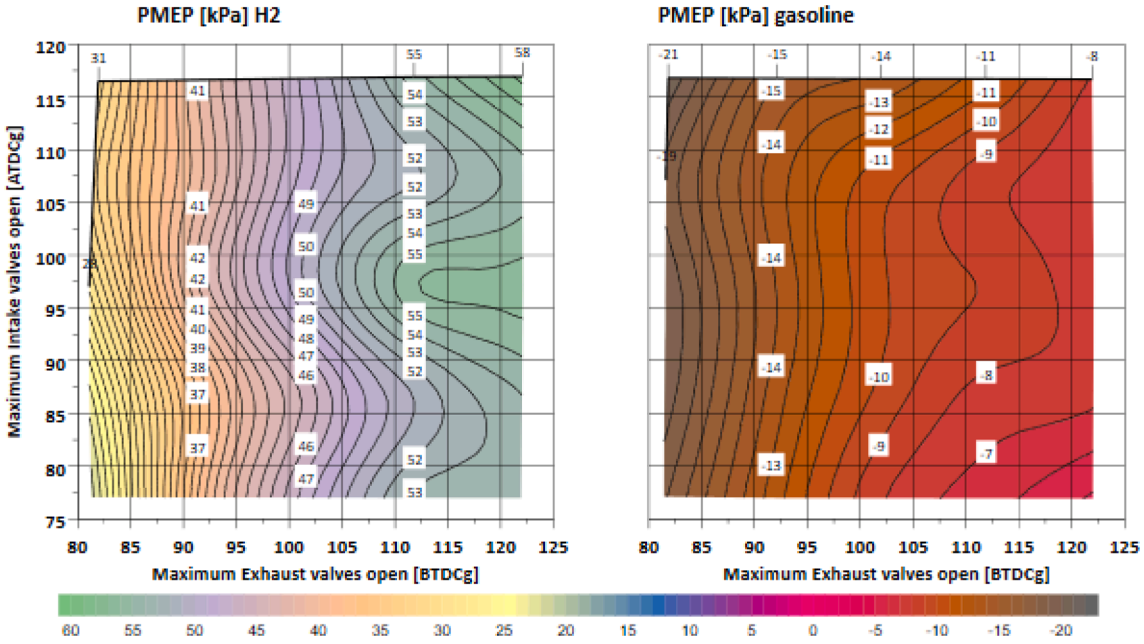

Fig. 10. The pumping mean effective pressure [KPa] for the hydrogen and gasoline at 10 bar IMEP and 2000 rpm.

the gasoline engine operation. The thermal efficiency of the hydrogen engine is almost independent of the valve timing and the valve overlap. The gasoline engine exhibits a slightly higher thermal efficiency with some valve overlap. Because of its much higher calorific value and higher thermal efficiency, the hydrogen ISFC is typically one-third of gasoline.

2- Despite the ultra-lean-burn mixture of Lambda 2.75, hydrogen combustion durations are only slightly longer than the stoichiometric combustion of gasoline. Additionally, the ultra-lean-burn hydrogen combustion is found to be as stable as the stoichiometric gasoline combustion. The combustion burn duration shows slightly higher dependency on the valve overlap for the hydrogen and higher dependency on the exhaust timing at the early intake open region for gasoline.

3- The ultra-lean burn hydrogen engine operation requires the use of boosted intake air supply and results in positive PEMP values whilst the gasoline engine is operating with a small negative PMEP at the 10 bar IMEP. It is found that less boosting for the hydrogen engine will be required when operated with a large valve overlap.

4- The standard emission analyzers could detect zero CO, CO_2, and HC emissions from the hydrogen engine operations. NO_x is the only emission in the hydrogen engine exhaust and it is mostly below 100 ppm and 15–20 times less than the gasoline engine. In the case of hydrogen engine operation, the maximum NO_x emission of 110 ppm is detected with the maximum valve overlap, whereas the gasoline NO_x engine-out emissions are lowest at 850 ppm in the maximum overlap region.

5- The H2 slip/emission is very low. The H2 slip increases with the more advanced intake valve opening and reaches its maximum of 660 ppm at the average exhaust opening time with a very early intake opening region. Similar trends can be seen for the unburnt HCs from the gasoline engine.

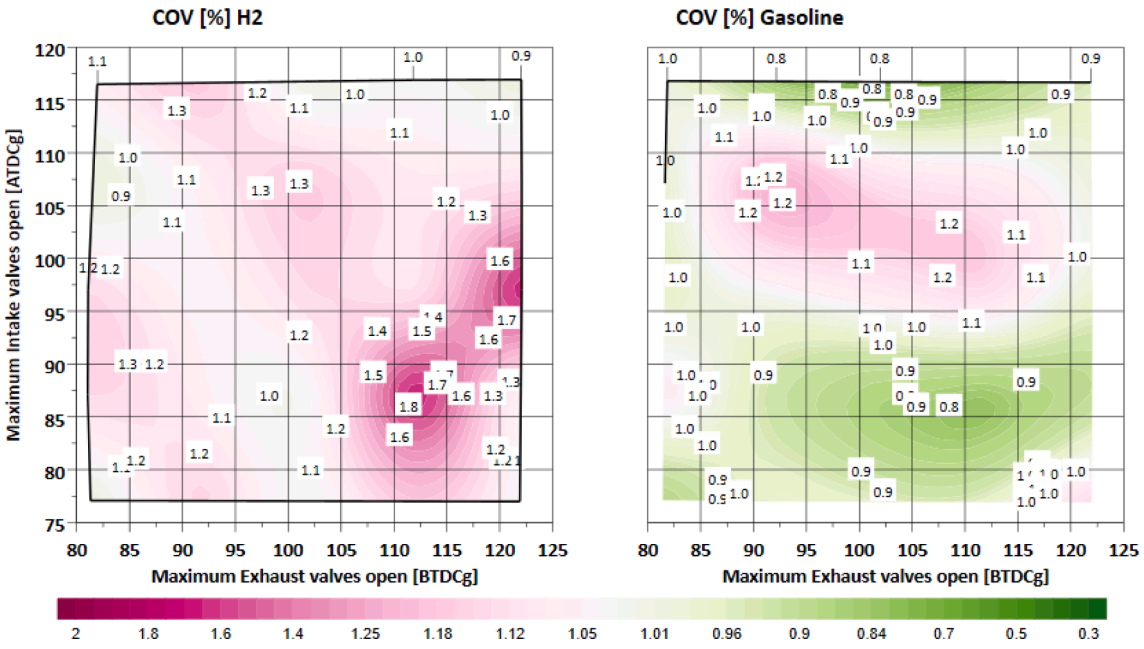

Fig. 11. The COV_{IMEP} [%] for the hydrogen and gasoline engines at 10 bar IMEP and 2000 rpm.

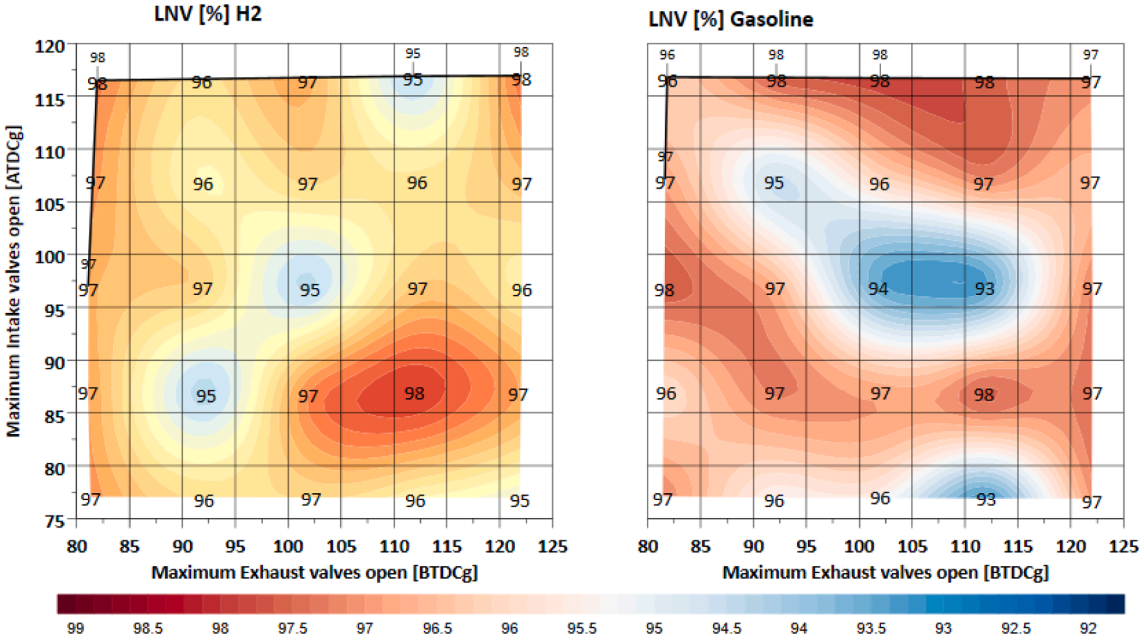

Fig. 12. The LNV [%] for the hydrogen and gasoline engines at 10 bar IMEP and 2000 rpm.

In conclusion, the research has demonstrated that a 4-stroke spark ignition gasoline engine can be readily adopted to operate with hydrogen, with significant significant benefits in terms of efficiency and emissions. Furthermore, the study has shown that adopting maximum valve overlap can substantially enhance engine performance without damaging hydrogen slips or backfires.

CRediT authorship contribution statement

Mohamed Mohamed: Data Curation, Visualization, Writing- original draft, Writing - review & editing. **Abinash Biswal:** Writing – original draft, Investigation. **Xinyan Wang:** Writing – review & editing, Validation, Supervision. **Hua Zhao:** Writing – review & editing, Supervision. **Jonathan Hall:** Validation, Project administration, Formal analysis, Conceptualization.

Declaration of competing interest

The authors declare that they have no known competing financial interests or personal relationships that could have appeared to influence the work reported in this paper.

Data availability

No data was used for the research described in the article.

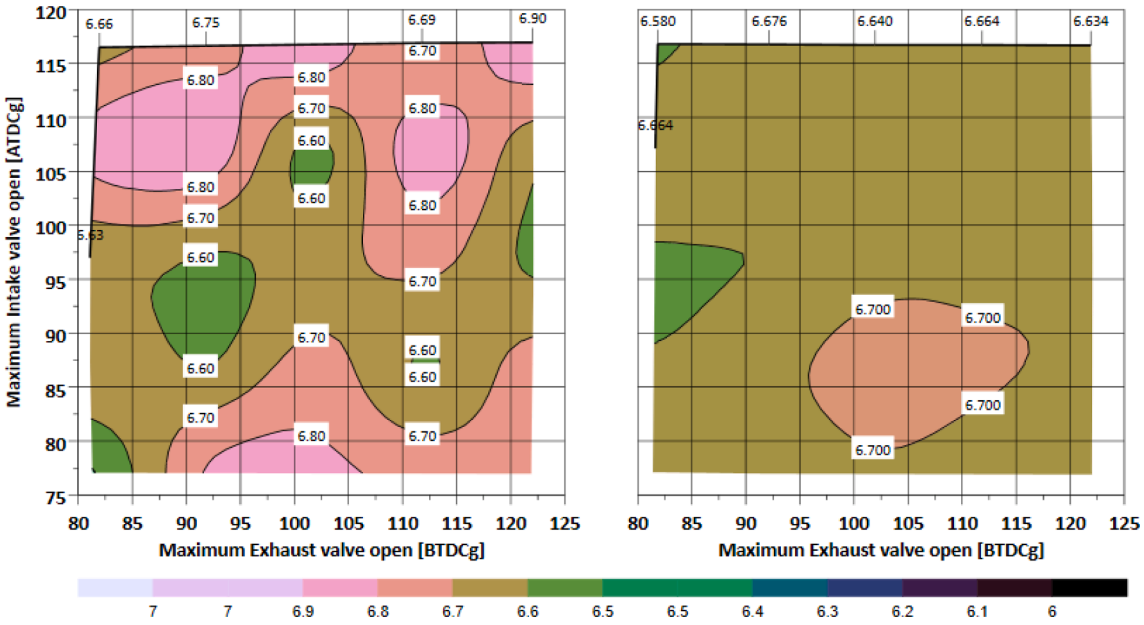

Fig. 13. The indicated power [kW] for the hydrogen and gasoline engines at 10 bar IMEP and 2000 rpm.

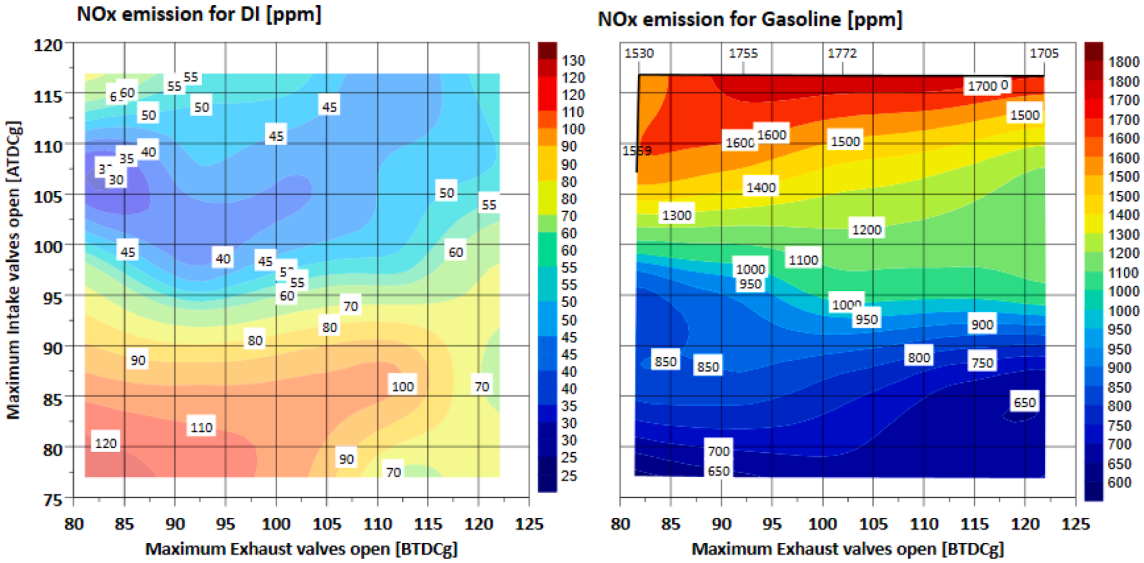

Fig. 14. The NO_x engine-out emissions [ppm] for the hydrogen and gasoline engines at 10 bar IMEP and 2000 rpm.

Appendix 1. Uncertainty in measurements

Measurement	Device	Manufacturer	Measurement range	Linearity/Accuracy
Engine speed	AC Dynamometers (Asynchronous)	Sierra Cp Engineering	0–6000 rpm	±1 rpm
Engine torque	AC Dynamometers (Asynchronous)	Sierra Cp Engineering	−50–500 nm	±0.25 % of FS
Clock Signal	EB582	Encoder Technology	0–25000 rpm	0.2 CAD
Hydrogen flowrate	Coriolis flowmeter K000000453	Alicate Scientific	0–10000 g/h	±0.20 % of reading
Intake air mass flow rate	F-106 AI	Bronkhust	4–200 kg/h	±0.2 % of reading
In-cylinder pressure	Piezoelectric pressure sensor Type 6125C	Kistler	0–30 MPa	≤±0.4 % of FS
Intake pressure	Piezoresistive pressure sensor Type 4049A	Kistler	0–1 MPa	≤±0.5 % of FS
exhaust pressure	Piezoresistive pressure sensor Type 4049B	Kistler	0–1 MPa	≤±0.5 % of FS
Oil pressure	PX309-10KGI	omega	0–0.8 MPa	<±0.2 % of FS
Temperature	Thermocouple K Type	RS	233–1473 K	≤±2.5 K
Fuel injector current signal	Current probe PR30	LEM	0–20 A	±2 mA
PM emissions	DMS 500	Cambustion	0–5000 PPS	–
CO emissions	MEXA-584L	Horiba	0–12 vol%	≤±1.0 % of FS or ± 2.0 % of readings
CO_2 emissions	MEXA-584L	Horiba	0–20 vol%	≤±1.0 % of FS or ± 2.0 % of readings
O2	MEXA-584L	Horiba	0–25 vol%	≤±1.0 % of FS or ± 2.0 % of readings

(*continued on next page*)

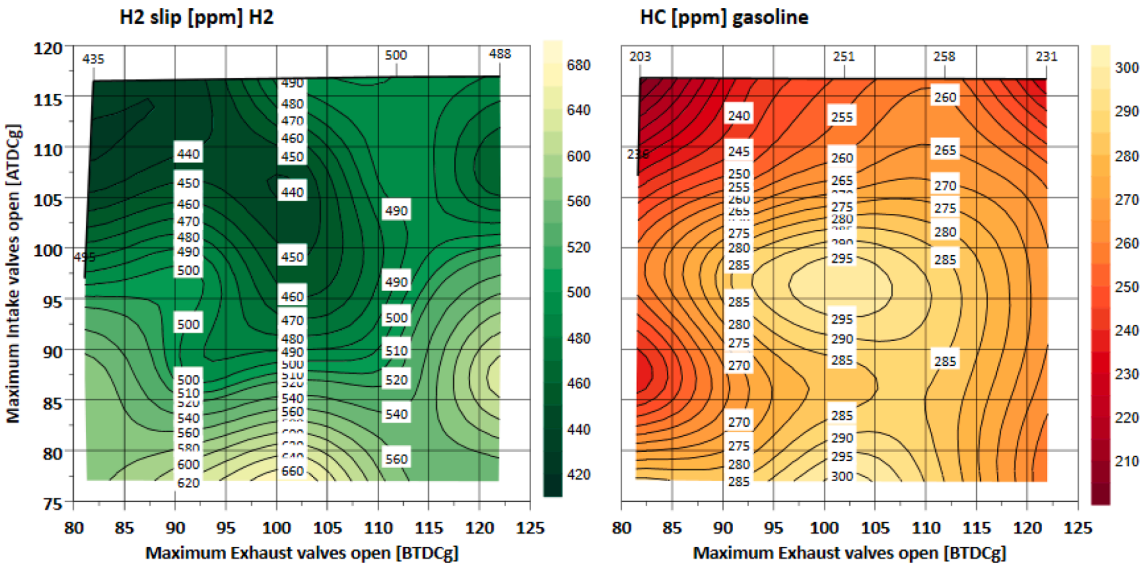

Fig. 15. Hydrogen slip vs gasoline unburnt hydrocarbon [ppm] for the hydrogen and gasoline at 10 bar IMEP and 2000 rpm.

(*continued*)

Measurement	Device	Manufacturer	Measurement range	Linearity/Accuracy
THC emissions	Rotork Analysis Model 523	Signal	0–5000 ppm	≤±1.0 % of FS or ± 2.0 % of readings
NO/NO2 emissions	CLD 150 (Heated Chemiluminescence Detector)	Cambustion	0–500 ppm or 0–10 k ppm	≤±1.0 % of FS or ± 2.0 % of readings
H2 slip emissions	Air sens500	V&F	0–5000 ppm or 0–100 % vol	0.5 % of fs or 1 %vol

Appendix 2. Injection PWM map

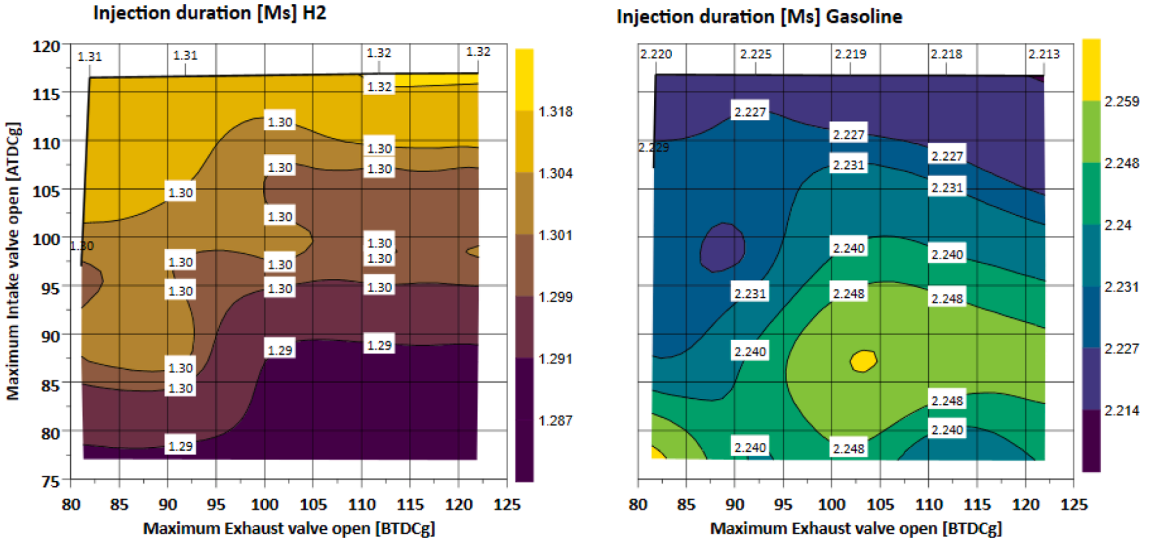

Fig. A1. Injection duration PWM [Ms].

References

[1] Chen Z, Wang L, Wei Z, Wang Y, Deng J. Effect of components on the emulsification characteristic of glucose solution emulsified heavy fuel oil. Energy 2022;244:123147. https://doi.org/10.1016/j.energy.2022.123147.

[2] Chen Z, Li K, Liu J, Wang X, Jiang S, Zhang C. Optimal design of glucose solution emulsified diesel and its effects on the performance and emissions of a diesel engine. Fuel 2015;157:9–15. https://doi.org/10.1016/j.fuel.2015.04.049.

[3] Wang X, Gao J, Chen H, Chen Z, Zhang P, Chen Z. Diesel/methanol dual-fuel combustion: an assessment of soot nanostructure and oxidation reactivity. Fuel Process Technol 2022;237:107464. https://doi.org/10.1016/j.fuproc.2022.107464.

[4] Wang J, Huang Z, Miao H, Wang X, Jiang D. Characteristics of direct injection combustion fuelled by natural gas–hydrogen mixtures using a constant volume vessel. Int J Hydrogen Energy 2008;33(7):1947–56. https://doi.org/10.1016/j.ijhydene.2008.01.007.

[5] Huang Z, Wang J, Liu B, Zeng K, Yu J, Jiang D. Combustion characteristics of a direct-injection engine fueled with natural gas–hydrogen blends under various injection timings. Energy Fuel 2006;20(4):1498–504. https://doi.org/10.1021/ef060032t.

[6] Huang Z, Wang J, Liu B, Zeng K, Yu J, Jiang D. Combustion characteristics of a direct-injection engine fueled with natural gas–hydrogen blends under different

ignition timings. Fuel 2007;86(3):381–7. https://doi.org/10.1016/j.fuel.2006.07.007.
[7] Ozcan H, El-Emam RS, Celik S, Amini Horri B. Recent advances, challenges, and prospects of electrochemical water-splitting technologies for net-zero transition. Clean Chem Eng 2023;8:100115. https://doi.org/10.1016/j.clce.2023.100115.
[8] Rosen MA, Koohi-Fayegh S. The prospects for hydrogen as an energy carrier: an overview of hydrogen energy and hydrogen energy systems. Energy Ecol Environ 2016;1(1):10–29. https://doi.org/10.1007/s40974-016-0005-z.
[9] Batra P. Alternative energy technologies: the unconventional dependable; 2015. doi: 10.4271/2015-24-2487.
[10] Climate Change and Net Zero: Public Awareness and Perceptions; 2021.
[11] Calvin K, et al. IPCC, 2023: climate change 2023: synthesis report. contribution of working groups I, II and III to the sixth assessment report of the intergovernmental panel on climate change [Core Writing Team, H. Lee and J. Romero (eds.)]. IPCC, Geneva, Switzerland; Jul. 2023. doi: 10.59327/IPCC/AR6-9789291691647.
[12] Onorati A, et al. The role of hydrogen for future internal combustion engines. Int J Engine Res 2022;23(4):529–40. https://doi.org/10.1177/14680874221081947.
[13] Yip HL, et al. A review of hydrogen direct injection for internal combustion engines: towards carbon-free combustion. Appl Sci 2019;9(22):4842. https://doi.org/10.3390/app9224842.
[14] Gao J, Tian G, Ma C, Balasubramanian D, Xing S, Jenner P. Numerical investigations of combustion and emissions characteristics of a novel small scale opposed rotary piston engine fuelled with hydrogen at wide open throttle and stoichiometric conditions. Energy Convers Manag 2020;221:113178. https://doi.org/10.1016/j.enconman.2020.113178.
[15] Ferrari A, Pizzo P. Injection technologies and mixture formation strategies for spark ignition and dual-fuel engines. SAE International; 2022.
[16] Welch A, et al. Challenges in developing hydrogen direct injection technology for internal combustion engines; Oct. 2008. doi: 10.4271/2008-01-2379.
[17] Verhelst S, Wallner T. Hydrogen-fueled internal combustion engines. Prog Energy Combust Sci 2009;35(6):490–527. https://doi.org/10.1016/j.pecs.2009.08.001.
[18] Lee S, Kim G, Bae C. Lean combustion of stratified hydrogen in a constant volume chamber. Fuel 2021;301:121045. https://doi.org/10.1016/j.fuel.2021.121045.
[19] Lad MR, Neveu JM, AKS. Development of medium duty H ₂ ICE for ON & OFF highway application; 2024. doi: 10.4271/2024-26-0170.
[20] Hu E, Xu Z, Gao Z, Xu J, Huang Z. Experimental and numerical study on laminar burning velocity of gasoline and gasoline surrogates. Fuel 2019;256:115933. https://doi.org/10.1016/j.fuel.2019.115933.
[21] Hu E, Huang Z, He J, Miao H. Experimental and numerical study on laminar burning velocities and flame instabilities of hydrogen–air mixtures at elevated pressures and temperatures. Int J Hydrogen Energy 2009;34(20):8741–55. https://doi.org/10.1016/j.ijhydene.2009.08.044.
[22] Huang Z, Zhang Y, Zeng K, Liu B, Wang Q, Jiang D. Measurements of laminar burning velocities for natural gas–hydrogen–air mixtures. Combust Flame 2006;146(1–2):302–11. https://doi.org/10.1016/j.combustflame.2006.03.003.
[23] Teoh YH, et al. A review on production and implementation of hydrogen as a green fuel in internal combustion engines. Fuel 2023;333:126525. https://doi.org/10.1016/j.fuel.2022.126525.
[24] Sahoo BB, Sahoo N, Saha UK. Effect of engine parameters and type of gaseous fuel on the performance of dual-fuel gas diesel engines—a critical review. Renew Sustain Energy Rev 2009;13(6–7):1151–84. https://doi.org/10.1016/j.rser.2008.08.003.
[25] Stern AG. Design of an efficient, high purity hydrogen generation apparatus and method for a sustainable, closed clean energy cycle. Int J Hydrogen Energy 2015;40(32):9885–906. https://doi.org/10.1016/j.ijhydene.2015.05.111.
[26] Chintala V, Subramanian KA. Experimental investigations on effect of different compression ratios on enhancement of maximum hydrogen energy share in a compression ignition engine under dual-fuel mode. Energy 2015;87:448–62. https://doi.org/10.1016/j.energy.2015.05.014.
[27] Møller KT, Jensen TR, Akiba E, Li H. Hydrogen - a sustainable energy carrier. Prog Nat Sci: Mater Int 2017;27(1):34–40. https://doi.org/10.1016/j.pnsc.2016.12.014.
[28] Shi W, Yu X, Zhang H, Li H. Effect of spark timing on combustion and emissions of a hydrogen direct injection stratified gasoline engine. Int J Hydrogen Energy 2017;42(8):5619–26. https://doi.org/10.1016/j.ijhydene.2016.02.060.
[29] Niu R, Yu X, Du Y, Xie H, Wu H, Sun Y. Effect of hydrogen proportion on lean burn performance of a dual fuel SI engine using hydrogen direct-injection. Fuel 2016;186:792–9. https://doi.org/10.1016/j.fuel.2016.09.021.
[30] Di Iorio S, Sementa P, Vaglieco BM. Analysis of combustion of methane and hydrogen–methane blends in small DI SI (direct injection spark ignition) engine using advanced diagnostics. Energy 2016;108:99–107. https://doi.org/10.1016/j.energy.2015.09.012.
[31] Sopena C, Diéguez PM, Sáinz D, Urroz JC, Guelbenzu E, Gandía LM. Conversion of a commercial spark ignition engine to run on hydrogen: performance comparison using hydrogen and gasoline. Int J Hydrogen Energy 2010;35(3):1420–9. https://doi.org/10.1016/j.ijhydene.2009.11.090.
[32] Lee J, Lee K, Lee J, Anh B. High power performance with zero NOx emission in a hydrogen-fueled spark ignition engine by valve timing and lean boosting. Fuel 2014;128:381–9. https://doi.org/10.1016/j.fuel.2014.03.010.
[33] Mohamed M, Zhao H, Harrington A, Hall J. Experimental investigation of combustion characteristics, performance, and emissions of a spark ignition engine with 2ndgeneration bio-gasoline and ethanol Fuels. SAE Technical Papers 2023. https://doi.org/10.4271/2023-01-0339.
[34] Mohamed M, Mirshahi M, Jiang C, Zhao H, Harrington A, Hall J. Hydrogen injection position impact: experimental analysis of central direct injection and side direct injection in engines. SAE Int J Engines 2024;17(5). https://doi.org/10.4271/03-17-05-0038. pp. 03–17-05–0038.
[35] "Vieletech - Vieletech Combustion Analysis Toolkit." Accessed: Mar. 03, 2024. [Online]. Available: https://www.vieletech.com/productdetails/VCAT.
[36] "MEXA-584L Automotive Emission Analyzer - HORIBA." Accessed: Nov. 20, 2023. [Online]. Available: https://www.horiba.com/gbr/automotive/products/detail/action/show/Product/mexa-584l-120/.
[37] "Fast Response Portable NO and NO2 Analyzer | CLD50." Accessed: Nov. 20, 2023. [Online]. Available: https://www.cambustion.com/products/engine-exhaust-emissions/nox-analyzers/cld50-ambient-and-engine-nox.
[38] V&F AirSense - V&F Analyse- und Messtechnik. Accessed: Nov. 20; 2023. [Online]. Available: https://www.vandf.com/en/products/analyzers/vf-airsense/.
[39] Mohamed M, Longo K, Zhao H, Hall J, Harrington A. Hydrogen engine insights: a comprehensive experimental examination of port fuel injection and direct injection. SAE Technical Paper Series Apr. 2024;1. https://doi.org/10.4271/2024-01-2611.
[40] Heywood JB. Internal combustion engine fundamentals. McGraw-Hill Education; 2018. Accessed: Apr. 27, 2024. [Online].
[41] Lewis B, von Elbe G. Combustion, flames and explosions of gases. Elsevier Science; 2012 [Online]. Available:.